RSC Advances

PAPER

View Article Online
View Journal | View Issue

Cite this: *RSC Adv.*, 2015, **5**, 32441

Porous membranes designed from bi-phasic polymeric blends containing silver decorated reduced graphene oxide synthesized *via* a facile one-pot approach

Prasanna Kumar S Mural,[a] Maya Sharma,[a] Abhinaya Shukla,[b] Sambhu Bhadra,[b] Babu Padmanabhan,[b] Giridhar Madras[c] and Suryasarathi Bose*[d]

In this work, porous membranes were designed by selectively etching the PEO phase, by water, from a melt-mixed PE/PEO blend. The pure water flux and the resistance across the membrane were systematically evaluated by employing an indigenously developed cross flow membrane setup. Both the phase morphology and the cross sectional morphology of the membranes was assessed by scanning electron microscopy and an attempt was made to correlate the observed morphology with the membrane performance. In order to design antibacterial membranes for water purification, partially reduced graphene oxide (rGO), silver nanoparticles (Ag) and silver nanoparticles decorated with rGO (rGO–Ag) were synthesized and incorporated directly into the blends during melt mixing. The loss of viability of bacterial cells was determined by the colony counting method using *E. coli* as a model bacterium. SEM images display that the direct contact with the rGO–Ag nanoparticles disrupts the cell membrane. In addition, the rGO–Ag nanoparticles exhibited a synergistic effect with respect to bacterial cell viability in comparison to both rGO and Ag nanoparticles. The possible mechanism associated with the antibacterial activity in the membranes was discussed. This study opens new avenues in designing antibacterial membranes for water purification.

Received 27th January 2015
Accepted 31st March 2015

DOI: 10.1039/c5ra01656h

www.rsc.org/advances

1 Introduction

The demand for pure water is a necessity in view of the rapidly increasing population, especially in developing nations. Fresh water conservation and purification of the existing sources has become indispensable in order to meet this global water demand. This requires better water management.[1] Among the various available water treatment technologies, such as media filtration, distillation or disinfection; separation technology is favored due to lower energy consumption, cost and it has no requirement for chemical additives.[1] Among the various membrane separation technologies, pressure driven separation is the most widely used method.[2,3]

Polymeric membranes are often used in the filtration technology due to their competitiveness in performance and economy.[4] Polymeric membranes are commercially prepared by various methods like thermally induced phase separation (TIPS), stretching melt-cast polymer films and track etching.[5] The polymeric membranes that are commercially available are made up of cellulose acetate, nitrocellulose, and cellulose esters, polysulfone, polyether sulfone, polyacrylonitrile, polyamide, polyimide, polypropylene, polytetrafluoroethylene, polyvinylidene fluoride and polyvinylchloride.[5] Among the different polymers that are commercially available, polyolefins are often of commercial interest due to their low, good processability and chemical resistance.[6]

Recently, Trifkovic *et al.*[7] generated porous structures by selectively etching one of the phases from bi-phasic polymeric blends. This method led to generation of porous structure with desired morphology and microstructure. Thus polymer blending offers myriad opportunities to design porous structures that can further be explored for separation technology. Polymer blends can, in general, be prepared either by solution mixing or by melt blending. The latter technique offers numerous advantage in designing new materials and hence an industrially viable technique.[8] It has been realized that blending two polymers often exhibit thermodynamic immiscibility, which leads to coarse morphology due to large interfacial tension between the phases.[9] Different morphologies such as droplet/matrix, fiber, lamella, and co-continuous are often

[a]*Center for Nano Science and Engineering, Indian Institute of Science, Bangalore-560012, India*

[b]*Polymer Science Diagnostic Center, Steer Engineering Pvt. Ltd, Bangalore-560058, India*

[c]*Department of Chemical Engineering, Indian Institute of Science, Bangalore-560012, India*

[d]*Department of Materials Engineering, Indian Institute of Science, Bangalore-560012, India. E-mail: sbose@materials.iisc.ernet.in*

obtained by blending and can be tuned by varying the physical properties like interfacial tension, viscosities, volume fractions and the processing parameters.[10] Among the different morphologies, the matrix/droplet morphology can be utilized for various applications, especially for separation technology by selectively removing the minor phase.

One of the major concerns in separation technology especially for water purification is that the membranes tend to foul over a period of time due to metabolic activities of the bacteria cells.[11–13] Fouling tends to decrease the permeate flux resulting in poor performance of the membrane. In recent years, nanoparticles such as graphene oxide (GO), silver (Ag), copper (Cu), zinc oxide (ZnO), and titanium oxide (TiO_2) *etc.*, have shown cytotoxicity to a broad spectrum of microorganisms.[14–16] However, studies related to the use of these nanoparticles in polymer matrix for membrane applications are still very scarce. GO sheets have sharp edges, which can physically damage the cell membrane leading to cell lysis.[17] Moreover, GO has a tendency to induce oxidative stress on the cell membrane.[18] On the other hand, Ag nanoparticles show antimicrobial activity[19] *via* release of silver ions (Ag^+) and the generation of reactive oxygen species (ROS).[13] It is well reported that the critical concentration for Ag nanoparticles that can kill bacterial cells is 0.001 μg L^{-1}.[20] However, Ma *et al.*[21] showed that Ag–GO composite powder can show very high bactericidal activity. This was attributed to the decrease in the surface charge that enhances the contact between the bacterial cell and the composite powder.

In this work, a unique strategy was adopted to design PE based porous membranes for water purification. PE/PEO (90/10, wt/wt) blends were melt mixed and the water soluble PEO phase was etched out to develop well defined porous structures. Pure water flux and the resistance across the membrane were evaluated using an indigenously developed cross flow cell. Different nanoparticles such as partially reduced graphene oxide (rGO), silver nanoparticles decorated rGO (rGO–Ag) were synthesized to impart antibacterial property to the membrane and more importantly, impede biofilm formation. The latter often results in clogging the pores and reduces the overall flux over a period of time. The efficacy of antibacterial activity was systematically assessed by using *Escherichia coli* (*E. coli*) as model bacterium. Further, the possible mechanisms associated with bacterial cell viability were also discussed.

2 Experimental

Materials

Low density polyethylene (PE with melt flow index of 25 g/10 min), polyethylene oxide (PEO, M_v of 400 000) was obtained from Sigma Aldrich. Silver nanoparticles and silver nitrate ($AgNO_3$) were procured from Merck (India). The size of the silver nanoparticles was *ca.* 20 nm. All other solvents and reagents were of analytical grade and were used as received.

Synthesis of graphene oxide (GO)

GO was synthesized by using an improved method as described in our previous work.[6] Briefly, graphite flakes were mixed with of concentrated H_2SO_4 and H_3PO_4 (9 : 1 ratio) in a water bath with the slow addition of $KMnO_4$ and the mixture was stirred for 24 h at room temperature. Upon completion of reaction, hydrogen peroxide was added to stop the reaction and then solution was filtered and washed successively with DI water, HCl and ethanol. Thus, the obtained solid (GO) was vacuum-dried at room temperature.

Synthesis of silver decorated partially reduced graphene oxide (rGO–Ag)

rGO–Ag was obtained by the method described elsewhere.[22] Briefly, 1 wt% of GO was added to ethylene glycol and sonicated for 30 min followed by 1 h of stirring. 200 mg of $AgNO_3$ was dissolved in a mixture of ethylene glycol and distilled water (DI). Thus obtained $AgNO_3$ mixture was added to GO–ethylene glycol mixture and the resultant solution was kept under constant stirring for 2 h at 50 °C. Further, $NaBH_4$ (40 mL of 0.1 mol L^{-1}) was added slowly and the mixture was heated to 110 °C and kept for 2 h under constant stirring. After completion of reaction, the mixture was washed and filtered using DI and then vacuum dried at 80 °C. In order to synthesize rGO, all the steps mentioned above were followed except the addition of $AgNO_3$, ethylene glycol and DI mixture.

Preparation of blends

Neat blends of PE/PEO (90/10 wt/wt) and with rGO, rGO–Ag nanoparticles were melt mixed using a twin screw extruder (Polylab, Thermo Haake Minilab II) at 150 °C and 60 rpm for 20 min under N_2 atmosphere. Homogeneous mixing was ensured by the recirculation channel in the Minilab II. Prior to mixing, all the samples were kept in a vacuum oven overnight to remove any traces of moisture. Blends were also prepared with GO and Ag.

Characterization of the nanoparticles

The characteristic dimensions of the synthesized nanoparticles were determined using field emission scanning electron microscopy (SEM) (ULTRA 55, FESEM, Carl Zeiss) with accelerating a voltage of 5 kV and transmission electron microscopy (TEM, Tecnai G2 T20). The presence of functional moieties was confirmed using spectroscopic techniques. Fourier transform infrared (FTIR) spectra were recorded on a Perkin-Elmer Frontier in the range of 400–4000 cm^{-1}. GO and rGO were further characterized using Raman spectroscopy using Horiba LabRAM HR with a 532 nm monochromatic laser. Diffraction patterns were acquired by X-ray diffraction (XRD) technique using a Rigaku Cu Kα source. X-ray Photon Scattering (XPS) was performed by Kratos Analytical instrument using Al monochromatic source.

The phase morphologies of the various blends and the cross sectional morphologies of the membranes were studied using cryo fractured surface by FESEM at 5 kV accelerating voltage. Prior to the morphological analysis, PEO was etched out with cold water to enhance the contrast between the phases. The mechanical properties of the blend was analyzed using uniaxial tensile test (as per ASTM D368 type V samples) using Instron

Universal Testing Machine at room temperature with a cross head speed of 5 mm min^{-1}. Surface wettability measurements and the contact angle measurements were performed using sessile drop water goniometry.

Membrane performance

The performance of the various membranes was analyzed by estimating the permeate flux (J) using an indigenously developed cross flow setup. Samples were hot pressed into discs and polished from both the sides as the flow properties of both PE and PEO are very different.[6] The following procedure was used to measure the pure water flux. The trans-membrane pressure was varied from 2.5 to 12.5 psi with a step change of 2.5 psi. It is important to mention here that prior to the measurements, the pressure was maintained for 30 min to obtain a steady flow and then the permeate flux was recorded. For stability and reproducibility of data at least three samples were tested. The experiments were repeated until three consecutive readings were within 10% of each reading. Permeate flux is defined as, $J = Q/A \times t$. Where Q (L) is the volume of permeated water, A (m^2) is area of the substrate and t (s) is the time taken by permeate to fill the volume (Q).

Antibacterial performance

The antibacterial activities of the membranes were evaluated using a wild culture of Gram-negative bacteria (*Escherichia coli*). Firstly, *E. coli* was sub cultured in Luria Bertani (LB) broth at 37 °C for 3 h (till mid log phase). Thus cultured *E. coli* was pelletized and washed with phosphate buffered saline (PBS) to remove nutrients from the broth. Pellets were re-suspended in PBS and diluted to reach the required concentration of 10^9 CFU mL^{-1}. The membranes of known dimensions were incubated in the PBS containing *E. coli* for 12 h. After 12 h, the *E. coli* cells were agar plated and the colonies formed after 24 h were assessed. The adhesion of the *E. coli* was analyzed by E-SEM. The samples were prepared by fixing the bacteria on the surface with 2.5% glutaraldehyde followed by rinsing by distilled water (DI) and dried under vacuum.

3 Results and discussion

Synthesis and characterization of GO, rGO and rGO–Ag

GO was synthesized using a modified Hummers method, where graphite was oxidized using $KMnO_4$ in the presence of H_2SO_4. The oxidation of graphite to GO was confirmed by using FTIR (Fig. 1) where a broad band centered around 3200 cm^{-1} is evident corresponding to the phenol hydroxyl groups on the basal plane. In addition, the characteristic stretching vibrations of the C=O (carboxylic) at 1726 cm^{-1}, the C=C sp^2 hybridization at 1626 cm^{-1} and the epoxide group at 1050 cm^{-1} further confirms the oxidation of graphite to GO.

Reduction of GO to rGO and Ag on to rGO[22] involves the use of ethylene glycol as a chelating and a mild reducing agent along with $NaBH_4$ (a strong reducing agent to enhance the rate of reaction). FTIR spectra of rGO–Ag indicates reduction in the intensities of hydroxyl and the carboxyl stretching which clearly

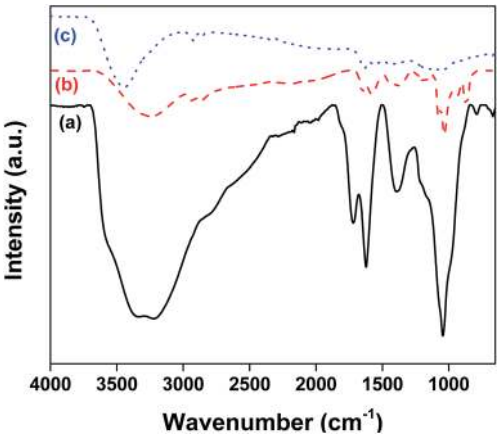

Fig. 1 FTIR spectra of (a) GO (b) rGO and (c) rGO–Ag.

manifests in the *in situ* reduction of GO in the presence of ethylene glycol and $NaBH_4$ during the synthesis of rGO–Ag. This presence of hydroxyl groups on the basal planes of GO is responsible for the interaction of Ag nanoparticles with the GO sheets.[22]

The Raman spectra of GO, rGO and rGO–Ag are shown in Fig. 2. From the spectra, it is well evident that the signature peaks of graphitic structures like D band (1333 cm^{-1}) and G band (1598 cm^{-1}) are present. The D band arises due to defects namely edge and disordered carbon. Similarly G band indicates the sp^2-bonded carbon *i.e.* graphitic structures. The ratio of intensities of D band (I_D) to G band (I_G) is indicative of degree of disorder and number of defects in the graphene sheet. For rGO, a slight increase in I_D/I_G ratio from 1.12 for GO to 1.15 is observed, which can be attributed to an increase in defects on account of reduction of oxygen sites. The I_D/I_G ratio increased further to 1.24, thus suggesting more defects in rGO–Ag, consistent with the literature.[22] It is envisaged that upon reduction of GO, the defects increases due to removal of the functional group and reduction of the sp^2 domains. Hence, an increase in I_D/I_G ratio is observed during reduction of GO.

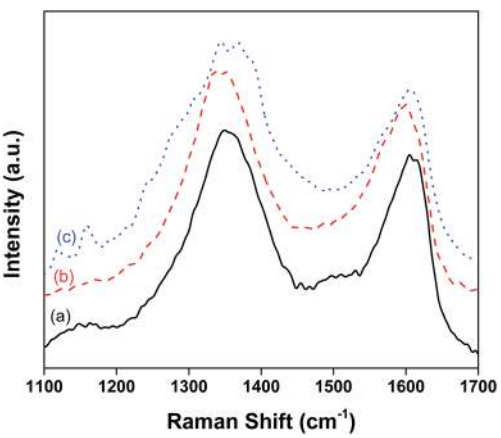

Fig. 2 Raman spectra of (a) GO (b) rGO and (c) rGO–Ag.

XRD (Fig. 3) of GO shows a peak at 10.19° 2θ and on reduction with ethylene glycol and $NaBH_4$, the peak centered around 20–30° can be attributed to the reflection of plane (002) of the hexagonal graphene sheet. This decrease in *d*-spacing and the broadening suggests re-stacking of graphene sheets[23] due to the reduction in oxygen groups. Further, rGO–Ag exhibited diffraction lines that can be indexed to Ag face centered cubic structure. The sharp peak at 38.2° suggests an average particle size of *ca.* 50 nm.

TEM micrograph (Fig. 4) of GO showed a thin, smooth surface along with minor wrinkles along the edges.[16] In case of rGO, a thick stack of sheets was observed that can be attributed to the removal of oxygen functional groups leading to the development of secondary bonding which is consistent with the results from XRD and FTIR. TEM micrograph of rGO–Ag clearly shows the deposition of Ag on the rGO sheets. These are marked by black dots on the surface and was confirmed from the diffraction pattern of the (111) plane of Ag.[21]

X-ray photon spectra (XPS) of GO and rGO–Ag are shown in Fig. 5. The presence of oxygen is well evident coming from various functional groups like carboxylic at the edge and the phenol hydroxyl and the epoxy groups on the basal plane. Upon reduction of Ag on the surface of GO, the corresponding intensities related to the oxygen species has decreased suggesting loss of oxygen groups during the reduction process. The rGO–Ag particles exhibited a doublet at 368.2 and 374.2 eV, which can be assigned to Ag $3d_{5/2}$ and Ad $3d_{3/2}$, respectively. Further, the splitting in 3d with a difference of 6.0 eV suggests the formation of metallic silver.[24] Interestingly, from the C/O ratios (Table 1), it is clear that the one-pot facile synthesis of rGO–Ag nanoparticles results in more oxygen species on the rGO sheets than the reduction of GO to rGO. From the above results, it is well evident that oxygen species provide nucleating sites for silver and further nucleation is strongly dependent on the degree of oxygen groups present on the surface.[25] It is well known phenomena that oxygen moieties are responsible for initial attachment of Ag^+ ions by electrostatic interactions. Further, upon reduction of Ag^+ ions using $NaBH_4$, the Ag particles grow on these sites. In the reduction of GO to rGO, the oxygen content has reduced in comparison to rGO–Ag nanoparticles which can be attributed to a competing effect. As reduction of Ag^+ by $NaBH_4$ is faster, the reduction of Ag is more favored than the reduction of functional groups in the GO sheet. It is further evident from XPS that rGO showed the highest C/O ratio (4.29) than rGO–Ag (1.93) supporting the above hypothesis. Further, presence of Ag on rGO–Ag will inhibit the restacking of GO sheet.[26] In case of rGO, the restacking of sheets due to strong van der Waals' forces[27] is indispensable and is also supported by TEM where rGO appears larger in size as compared to GO. Interestingly, the rGO–Ag nanoparticles are smaller in size than the rGO sheets possibly due to fragmentation of the sheets during the synthesis of rGO–Ag nanoparticles.

It is important to note that the Ag nanoparticles did not get oxidized during the preparation of rGO–Ag. To support this hypothesis, XRD was carried out on the rGO–Ag powder which was exposed to air atmosphere for 24 h and on the membrane tokens containing rGO–Ag which was exposed to water for one month (not shown here). Interestingly, we observed identical diffraction patterns for the membrane tokens with 1 wt% rGO–Ag after exposing the membranes to water for a months' time with respect to the as prepared membrane tokens. Similar observations were recorded for the nanoparticles which were exposed to air. This clearly demonstrates the fact that Ag do not oxidize in rGO–Ag nanoparticles.

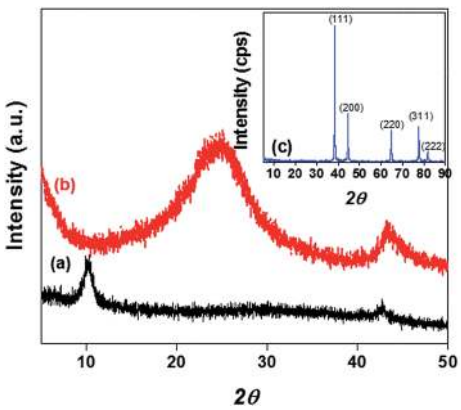

Fig. 3 XRD patterns of (a) GO (b) rGO and (c) rGO–Ag nanoparticles.

Phase morphology in PE/PEO blends

The phase morphology in the blends depends on various parameters such as blend ratio, melt viscosity, processing parameters and also on the presence of nanoparticles *etc.*[28] PE/PEO blends form an immiscible pair and offer different morphologies depending on the viscosity ratio of the constituent polymers.[6,7,29,30] Fig. 6 displays the SEM micrographs of various blends generated by blending PE (90 wt%) and PEO (10 wt%). The minor phase (*i.e.* PEO) has been etched out with water to enhance the contrast between the phases and hence, the holes in the micrographs represents the etched out PEO phase. The average pore size in the neat blends is of the order of 1.3 μm.[6] Further, with addition of rGO, Ag and rGO–Ag particles a marginal decrease in pore size is observed, which can be due to suppression of coalescence led by the nanoparticles. It is well known that nanoparticles can either increase the viscosity of the matrix phase or can act as a physical barrier between the droplets.[31] The nanoparticles selectively localize in the PE phase of the blends, driven by its lower melt viscosity in striking contrast to PEO. This is evident from the SEM micrographs (see inset of Fig. 6d) where rGO–Ag nanoparticles appear as bright features marked by wrinkled edges. This droplet-matrix morphology, thus generated by blending PE and PEO, can be further explored for membrane separation application and is discussed in the next section.

Membrane performance

The trans-membrane flux across the membranes was determined using a typical cross flow setup. Prior to the flux measurements, the membranes were prepared by polishing the surface to a depth of 200 nm. This was done to remove the skin

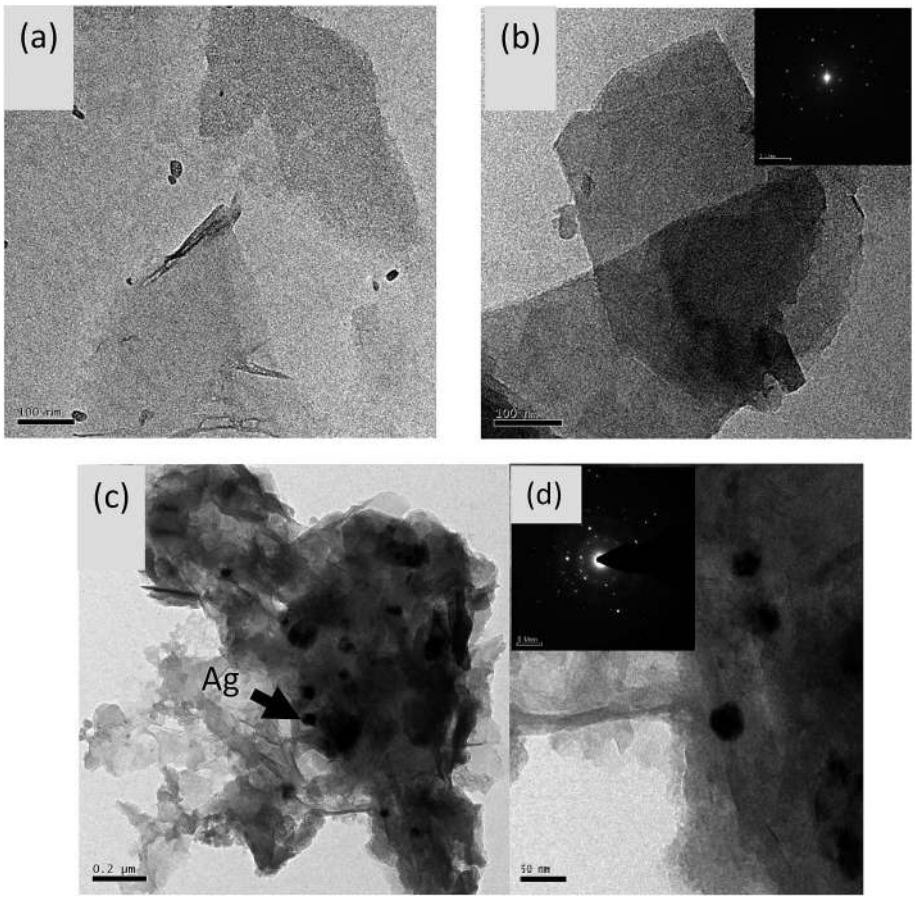

Fig. 4 TEM micrographs of (a) GO (b) rGO (c) rGO–Ag and (d) higher magnification micrograph of rGO–Ag (inset shows the corresponding diffraction patterns).

layer, which is PE rich as explained in detail in our previous work.[6] Fig. 7 represents the typical flux measurements as a function of trans-membrane pressure. It is clear from Fig. 7 that incorporation of different nanoparticles has decreased the flux across the membrane and can be attributed to decrease in the pore size. This is also supported by the observed morphological changes, as discussed in the previous section.

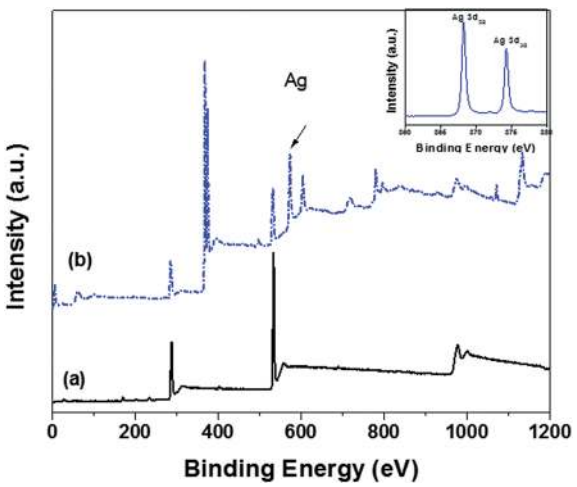

Fig. 5 XPS spectra of (a) GO and (b) rGO–Ag (inset shows Ag 3d elemental scan).

The resistance offered by the membrane was measured from the reciprocal of slope in Fig. 7. From Table 2 it is clear that with the incorporation of particles the resistance offered by the membranes has increased from 9.02 ± 0.11 psi $(\mathrm{L\ m^{-2}\ h^{-1}})^{-1}$ for neat blends to 29.43 ± 0.43 psi $(\mathrm{L\ m^{-2}\ h^{-1}})^{-1}$ with incorporation of rGO–Ag. This clearly suggests a decrease in the pore size resulting from suppression of coalescence. The particles present in the matrix act as a physical barrier thereby prevents droplet coalescence and stabilizes the blend morphology. This reduction in droplet offers higher resistance to the flow which results in an increase in the resistance to flow and decreases the overall flux. Vleminckx *et al.*[32] reported that coarsening of the domain in matrix was suppressed by TRG (thermally reduced graphene) which acts as physical barrier in the blend. Table 2 also depicts the contact angle of the various membranes. The contact angle for blends with GO is *ca.* 59 ± 2 and can be attributed to various functional groups present on the surface. These surface oxygen groups are substantially reduced in the blends with rGO thereby, making it more hydrophobic.

In order to check the compaction in the membrane tokens, we had pressurized the tokens to 10 psi and stabilized it for 1 h and subsequently the pressure was reduced to half and the flux

Table 1 XPS of GO, rGO and rGO–Ag nanoparticles

Particle	Elements	Atomic concentration (%)	Mass concentration (%)	C/O ratio (atomic ratio)
GO	C	61.6	55.0	1.61
	O	38.4	45.0	
rGO	C	81.1	76.3	4.3
	O	18.9	23.7	
rGO–Ag	C	55.3	23.7	2.0
	O	28.8	16.3	
	Ag	15.7	60.0	

was measured as *ca.* 637.02 ± 8.18 L m^{-2} h^{-1}. Prior to these measurements, we initially measured the flux at 5 psi which showed *ca.* 644.89 ± 39.03 L m^{-2} h^{-1}. These observations clearly demonstrate the fact that the compaction phenomenon is not pronounced in PE/PEO blends.

Antibacterial activity in the membranes: effect of rGO and rGO–Ag nanoparticles

The antibacterial activity of the membranes was evaluated using *E. coli.*(Gram-negative) as a model bacterium. The antibacterial activity after 24 h in terms of CFU mL^{-1} of neat, rGO, Ag, and rGO–Ag membranes is shown in Fig. 8. Compared to the membranes derived from neat blends, the membranes with 1 wt% rGO, Ag and rGO–Ag exhibited significantly higher bactericidal effect as observed from the plates where only fewer colonies of *E. coli* was present.

It is envisaged that rGO can lead to cell death due to oxidative stress or physical disruption causing rupture of cell wall.[27] In the present study, the mechanism of physical disruption causing rupture of cell is studied in further detail by SEM and will be discussed in the subsequent section. Fig. 9 shows the

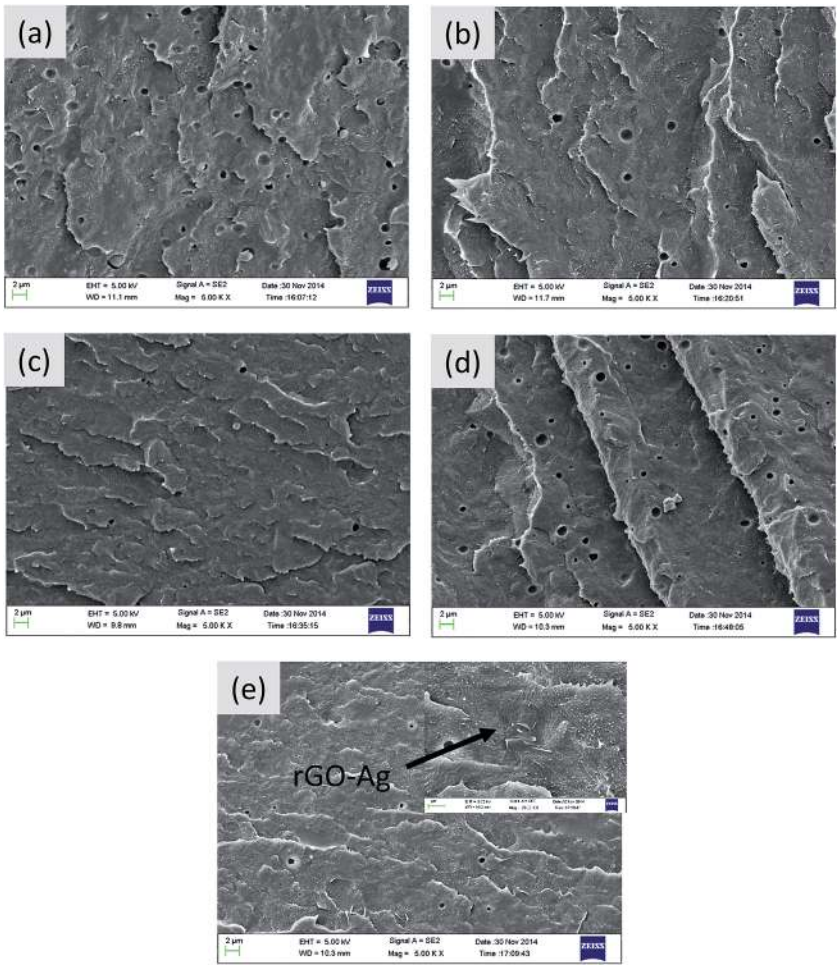

Fig. 6 Morphology of 90/10 PE/PEO blends (a) neat (b) with 1 wt% GO (c) with 1 wt% rGO, (d) with 1 wt% Ag and (e) with 1 wt% rGO–Ag (inset shows the higher magnification of 90/10 PE/PEO blend with 1 wt% rGO–Ag).

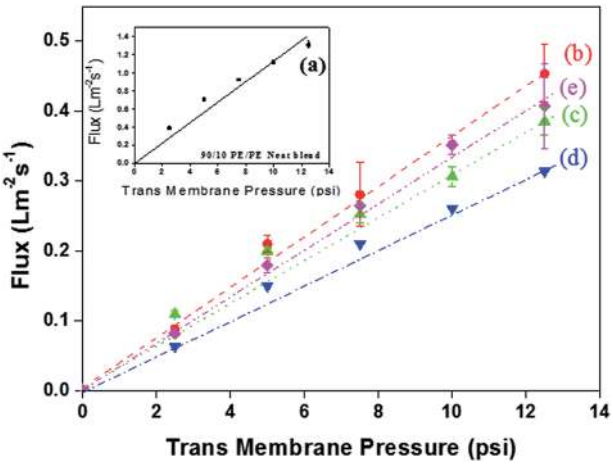

Fig. 7 Typical flux measurement *versus* trans membrane pressure of 90/10 PE/PEO blends (a) neat (b) with 1 wt% GO (c) with 1 wt% rGO, (d) with 1 wt% Ag and (e) with 1 wt% rGO–Ag.

Table 2 Contact angle, resistance and flux across the membranes

Sample	Contact angle (°)	Resistance (psi L^{-1} m^2 s)	Avg. flux@12.5 psi (L m^{-2} h^{-1})
Neat	75 ± 2	9.02 ± 0.25	4721 ± 134
With 1 wt% GO	59 ± 2	27.34 ± 2.46	1633 ± 147
With 1 wt% rGO	75 ± 3	31.12 ± 1.57	1386 ± 70
With 1 wt% Ag	69 ± 3	38.18 ± 2.98	1243 ± 97
With 1 wt% rGO–Ag	77 ± 2	29.43 ± 1.66	1365 ± 77

agar plates after inoculation of *E. coli* for 12 h. It is clear from these plates that in the case of rGO, the cell count has decreased from 3×10^8 to 1.2×10^8 CFU mL^{-1}. Similarly, in the case of Ag nanoparticles, a significant decrease in the CFU mL^{-1} was noted. This can be attributed to the disruption of cell membrane function, which can interrupt the electron transport system and further damage the cell proteins and DNA (by binding to sulphur group like thiol group).[33] This is also well supported by SEM and will be discussed in the subsequent section. Such a slow rate may be due to slow release of Ag ions from the membranes in the PBS media.[33] Muñoz-Bonilla *et al.*[34] recently highlighted that the release of Ag ions is more in hydrophilic polyamide nanocomposites than in hydrophobic polypropylene. In addition, they reported that the slow release of Ag ions will have long term antibacterial behavior. Interestingly, in the membranes with rGO–Ag a synergistic effect was noted. The CFU mL^{-1} further decreased to 7.5×10^7 cells. Ma *et al.*[21] showed that rGO–Ag showed a decrease in the negative charge in comparison with GO. This reduction in surface charge enhances the contact between the particle and the *E. coli* cells. We believe that the direct contact of rGO–Ag nanoparticles with *E. coli* results in synergistic effects in the membrane. This will impede the formation of biofilm formation on the membrane. Sharma *et al.*[35] recently reported a similar phenomenon in PDVF membrane wherein the biofilm was prevented by incorporation of Ag nanoparticles.

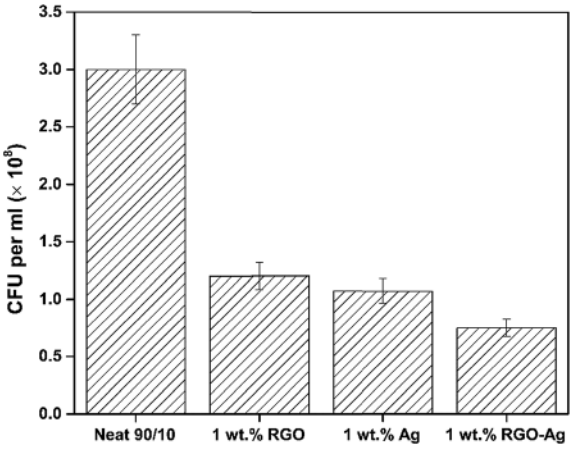

Fig. 8 Dependence of CFU mL^{-1} on the composition of the composites after 12 h of inoculation.

Cell viability

The morphological changes in *E. coli*, when exposed to the membranes, are displayed in Fig. 10. The membranes derived from neat 90/10 PE/PEO blends exhibited a smooth and intact *E. coli* cells (Fig. 10a) whereas the membranes with the nanoparticles showed disturbed and flattened morphology. From Fig. 10b it is well evident that the sharp edges of rGO might have resulted in disruption of the cell membrane leading to its death. This physical disruption of cell membrane in the presence of rGO can be explained in terms of the nature of the cell. The Gram negative bacteria cells have a thin layer of peptidoglycan of *ca.* 7–8 nm along with a layer of lipopolysaccharides.[36] This peptidoglycan can interact with the rGO sheets. Further, sharp edges of rGO can also disrupt the cell membrane leading to the release of intracellular content (debris). This physical disruption of peptidoglycan leads to lysis of cells.[17]

Recently, several studies have comprehensively highlighted the bactericidal properties of silver nanoparticles.[37,38] Fig. 10c shows the cell morphology in the presence of membranes with Ag nanoparticles. Several mechanisms have been proposed for the loss of cell viability in the presence of Ag. In the present study, from the SEM micrographs, it is evident that due to direct contact with the cells Ag nanoparticles has led to irreversible cell damage finally resulting in cell death. However in the case of rGO–Ag nanoparticles, we believe that the adsorption is much stronger due to decrease in the negative charge, as compared to GO, (refer inset of Fig. 10d). This adsorption prevents bacterial cell nourishment. In addition, direct contact with rGO–Ag might also induce membrane stress resulting in cell lysis. The Gram negative bacteria (such as the one studied here, *E. coli*) comprise cell wall of thin layer of peptidoglycan (PG) and an outer membrane consisting of lipopolysaccharides. The latter gives negative charge to the cell membrane which is essential for its structural integrity and viability.[39] Thus, if the structural integrity of the cell is disturbed then the viability of the cell is lost resulting in cell lysis. The bactericidal effects associated with rGO has been reported with respect to its size,

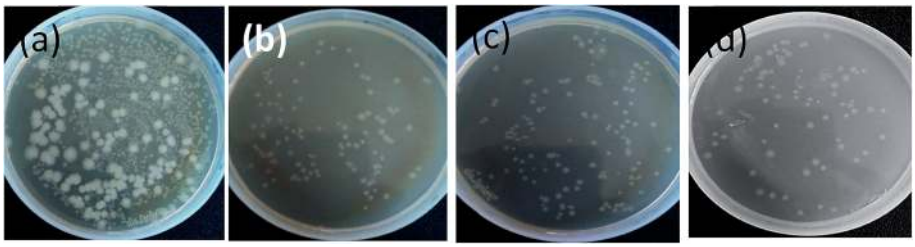

Fig. 9 Antibacterial properties of the composites shown on total agar plate counts. The number of bacterial colonies that appear on the agar plate, relative to the control, after 12 h of inoculation for 90/10 PE/PEO (a) neat blends (b) with 1 wt% rGO (c) with 1 wt% Ag and (d) with 1 wt% rGO–Ag.

oxidation capacity, physical disruption of membrane or by bridging lipid bilayer to external environment for release of cellular energy.[40] GO, due to presence of oxygen group on the surface are insulators and hence can bridging lipid bilayer to external environment for the release of cellular energy is impeded as against rGO, which are conducting. The rGO sheets are capable of interacting with thick cell membrane and the sharp edges disrupts the cell membrane leading to the release of intracellular content and finally resulting in irreversible cell lysis.

Silver nanoparticles disrupts the permeability, respiration, and cell division when it interacts with the cell membrane and the sulfur- and phosphorus-containing compounds.[41] It also depends on various factors like particle size, shape and water chemistry.[40] Smaller particle size enhances the antibacterial properties due to high specific surface area.[41]

Interestingly, the rGO–Ag nanoparticles showed synergistic effect in bactericidal properties. This can be attributed to slight positive charge on rGO–Ag as compared to rGO.[21] To support our hypothesis, zeta potential for GO, rGO and rGO–Ag was estimated using the zeta potential (-27.4 ± 0.3 mV at 7 pH in distilled water) of Ag as the reference. We observed that GO, rGO and rGO–Ag, showed a zeta potential of -40.28 ± 1.56, -34.44 ± 1.33 and -29.27 ± 1.78 mV respectively, at pH 7. This decrease in zeta potential of rGO–Ag suggests that rGO–Ag exhibit a relatively positive charge and can be attributed to the decrease in functional group and incorporation of positively charged Ag nanoparticles. Hence from zeta potential, we can argue that rGO–Ag possess a positive charge on the surface and this charge is responsible for physiological interaction between the negatively charged lipopolysaccharides and the rGO–Ag nanoparticles leading to cell death.[41] In addition, the rGO–Ag

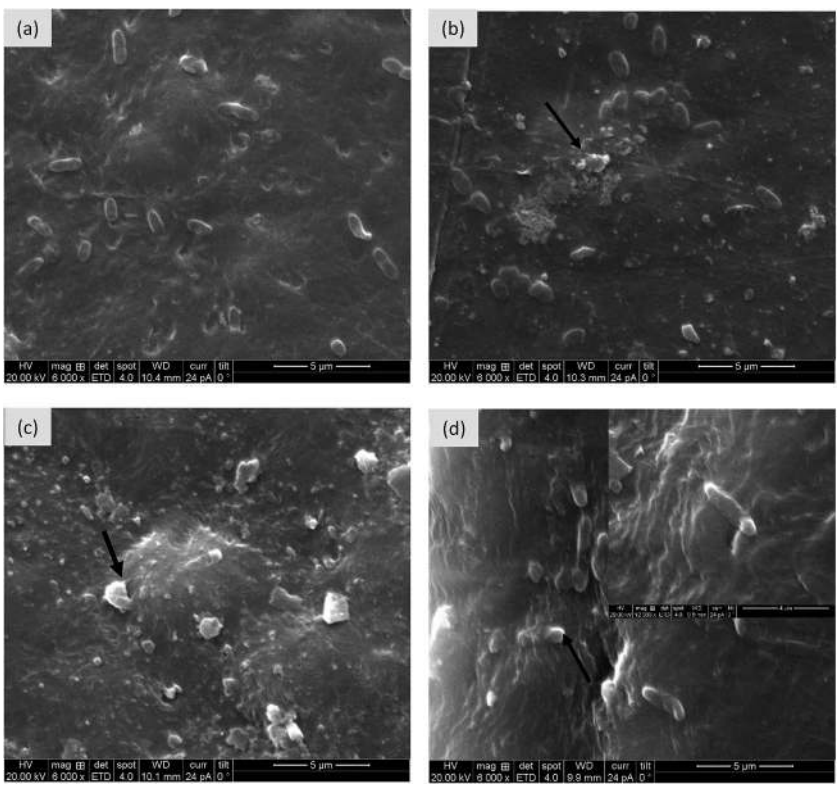

Fig. 10 Morphological of 90/10 PE/PEO (a) neat (b) with 1 wt% rGO (c) with 1 wt% Ag and (d) with 1 wt% rGO–Ag (arrows indicate cell lysis).

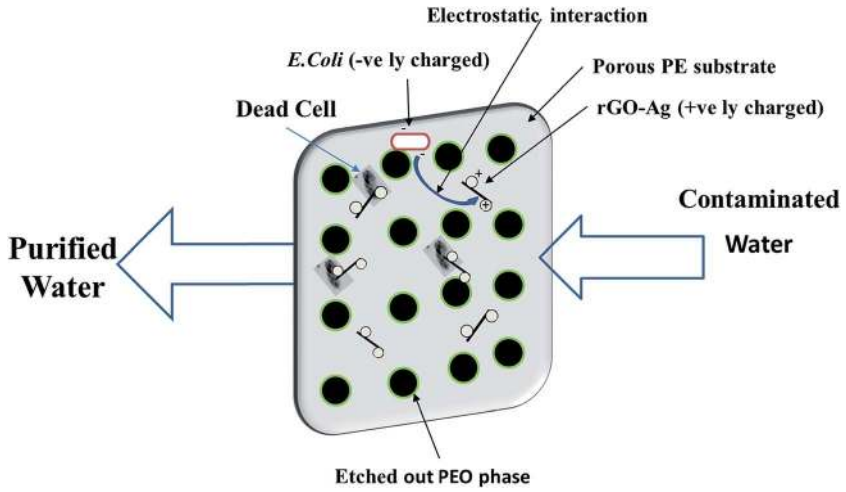

Fig. 11 A cartoon illustrating the key role of rGO–Ag nanoparticles as bactericidal agent in porous PE membranes for water purification.

nanoparticles exhibited fragmented graphene sheets, as observed in TEM, with sharp edges which can physical disrupt the membrane. As discussed earlier, the oxygen content in rGO–Ag nanoparticles are higher with respect to rGO. This higher content of oxygen species possibly can impart oxidative stress on the cell membrane. It is worth mentioning that we mapped the release of Ag ions from the membranes by AAS (atomic absorption spectroscopy) over a period of 12 h to understand the release kinetics (not shown here). We did not observe any appreciable release of Ag ions that clearly indicates that the bactericidal effects in Ag nanoparticles are *via* direct contact. This observation can also possibly explain the similar bactericidal effects noted in both Ag and rGO nanoparticles. The factors discussed above explain the synergistic effects in rGO–Ag nanoparticles. An important observation is worth pointing out here. The bactericidal effects rendered by rGO–Ag can possibly impede the biofilm formation. The latter often results in clogging the pores and lead to overall decrease in the flux. Sharma *et al.*[35] recently reported a similar phenomenon in PDVF membrane wherein the biofilm was prevented by incorporation of Ag nanoparticles. It is envisaged that in PE based membranes, the biofilm formation is the major cause for degradation. Hence, by preventing this, the lifetime of the proposed membranes can be enhanced significantly and a detailed investigation in this regard is subjected to future investigation. A cartoon further highlighting the conceptual design of antibacterial membranes is displayed in Fig. 11.

4 Conclusions

A unique strategy was adopted to design antibacterial membranes in this study. By etching out one of the phases from a binary blend, porous substrates were developed and evaluated for membrane performance. Both the cross section and the phase morphology was corroborated with the observed flux and the resistance offered by the membranes. The effect of rGO, Ag and Ag decorated rGO was evaluated on the bactericidal effect on the membrane. The membranes with rGO–Ag showed synergistic improvement in the bactericidal activity against *E. coli*. Such membranes can open up new avenues for water purification using a cost effective and easy to process PE based membranes.

Acknowledgements

The authors would like to acknowledge the Department of Science and Technology for the financial support, Prof. Jayant Modak for extending his facilities and Materials Engineering Department and CeNSE, IISc for various characterization facility.

References

1 M. M. Pendergast and E. M. V. Hoek, A review of water treatment membrane nanotechnologies, *Energy Environ. Sci.*, 2011, **4**, 1946–1971.
2 R. E. Kesting, The four tiers of structure in integrally skinned phase inversion membranes and their relevance to the various separation regimes, *J. Appl. Polym. Sci.*, 1990, **41**, 2739–2752.
3 M. Ulbricht, Advanced functional polymer membranes, *Polymer*, 2006, **47**, 2217–2262.
4 A. Mehta and A. L. Zydney, Permeability and selectivity analysis for ultrafiltration membranes, *J. Membr. Sci.*, 2005, **249**, 245–249.
5 G. M. Geise, H.-S. Lee, D. J. Miller, B. D. Freeman, J. E. McGrath and D. R. Paul, Water purification by membranes: the role of polymer science, *J. Polym. Sci., Part B: Polym. Phys.*, 2010, **48**, 1685–1718.
6 P. K. S. Mural, A. Banerjee, M. S. Rana, A. Shukla, B. Padmanabhan, S. Bhadra, G. Madras and S. Bose, Polyolefin based antibacterial membranes derived from PE/PEO blends compatibilized with amine terminated graphene oxide and maleated PE, *J. Mater. Chem. A*, 2014, **2**, 17635–17648.

7 M. Trifkovic, A. Hedegaard, K. Huston, M. Sheikhzadeh and C. W. Macosko, Porous Films *via* PE/PEO Cocontinuous Blends, *Macromolecules*, 2012, **45**, 6036–6044.
8 S. Bose, A. R. Bhattacharyya, A. R. Kulkarni and P. Pötschke, Electrical, rheological and morphological studies in co-continuous blends of polyamide 6 and acrylonitrile–butadiene–styrene with multiwall carbon nanotubes prepared by melt blending, *Compos. Sci. Technol.*, 2009, **69**, 365–372.
9 L. A. Utracki, *Polymer blends handbook*, Kluwer Academic Publishers, Dordrecht, The Netherlands, 2002.
10 C. L. Tucker and P. Moldenaers, Microstructural evolution in polymer blends, *Annu. Rev. Fluid Mech.*, 2002, **34**, 177–210.
11 J. Brame, Q. Li and P. J. Alvarez, Nanotechnology-enabled water treatment and reuse: emerging opportunities and challenges for developing countries, *Trends Food Sci. Technol.*, 2011, **22**, 618–624.
12 J. Huang, G. Arthanareeswaran and K. Zhang, Effect of silver loaded sodium zirconium phosphate (nanoAgZ) nanoparticles incorporation on PES membrane performance, *Desalination*, 2012, **285**, 100–107.
13 D. Y. Koseoglu-Imer, B. Kose, M. Altinbas and I. Koyuncu, The production of polysulfone (PS) membrane with silver nanoparticles (AgNP): physical properties, filtration performances, and biofouling resistances of membranes, *J. Membr. Sci.*, 2013, **428**, 620–628.
14 A. Agarwal, T. L. Weis, M. J. Schurr, N. G. Faith, C. J. Czuprynski, J. F. McAnulty, C. J. Murphy and N. L. Abbott, Surfaces modified with nanometer-thick silver-impregnated polymeric films that kill bacteria but support growth of mammalian cells, *Biomaterials*, 2010, **31**, 680–690.
15 Q. Bao, D. Zhang and P. Qi, Synthesis and characterization of silver nanoparticle and graphene oxide nanosheet composites as a bactericidal agent for water disinfection, *J. Colloid Interface Sci.*, 2011, **360**, 463–470.
16 J. Chen, H. Peng, X. Wang, F. Shao, Z. Yuan and H. Han, Graphene oxide exhibits broad-spectrum antimicrobial activity against bacterial phytopathogens and fungal conidia by intertwining and membrane perturbation, *Nanoscale*, 2014, **6**, 1879–1889.
17 H. N. Abdelhamid, M. S. Khan and H.-F. Wu, Graphene oxide as a nanocarrier for gramicidin (GOGD) for high antibacterial performance, *RSC Adv.*, 2014, **4**, 50035–50046.
18 H. Zhang, D. Yee and C. Wang, Quantum dots for cancer diagnosis and therapy: biological and clinical perspectives, *Nanomedicine*, 2008, **3**, 83–91.
19 T. Maneerung, S. Tokura and R. Rujiravanit, Impregnation of silver nanoparticles into bacterial cellulose for antimicrobial wound dressing, *Carbohydr. Polym.*, 2008, **72**, 43–51.
20 M. Toroghi, A. Raisi and A. Aroujalian, Preparation and characterization of polyethersulfone/silver nanocomposite ultrafiltration membrane for antibacterial applications, *Polym. Adv. Technol.*, 2014, **25**, 711–722.
21 J. Ma, J. Zhang, Z. Xiong, Y. Yong and X. Zhao, Preparation, characterization and antibacterial properties of silver-modified graphene oxide, *J. Mater. Chem.*, 2011, **21**, 3350–3352.
22 Y. Shen, T. Jing, W. Ren, J. Zhang, Z.-G. Jiang, Z.-Z. Yu and A. Dasari, Chemical and thermal reduction of graphene oxide and its electrically conductive polylactic acid nanocomposites, *Compos. Sci. Technol.*, 2012, **72**, 1430–1435.
23 C. Xu and X. Wang, Fabrication of Flexible Metal-Nanoparticle Films Using Graphene Oxide Sheets as Substrates, *Small*, 2009, **5**, 2212–2217.
24 C.-N. Lok, C.-M. Ho, R. Chen, Q.-Y. He, W.-Y. Yu, H. Sun, P.-H. Tam, J.-F. Chiu and C.-M. Che, Silver nanoparticles: partial oxidation and antibacterial activities, *J. Biol. Inorg. Chem.*, 2007, **12**, 527–534.
25 G. Goncalves, P. A. A. P. Marques, C. M. Granadeiro, H. I. S. Nogueira, M. K. Singh and J. Grácio, Surface Modification of Graphene Nanosheets with Gold Nanoparticles: The Role of Oxygen Moieties at Graphene Surface on Gold Nucleation and Growth, *Chem. Mater.*, 2009, **21**, 4796–4802.
26 Y. Si and E. T. Samulski, Exfoliated Graphene Separated by Platinum Nanoparticles, *Chem. Mater.*, 2008, **20**, 6792–6797.
27 S. Liu, T. H. Zeng, M. Hofmann, E. Burcombe, J. Wei, R. Jiang, J. Kong and Y. Chen, Antibacterial activity of graphite, graphite oxide, graphene oxide, and reduced graphene oxide: membrane and oxidative stress, *ACS Nano*, 2011, **5**, 6971–6980.
28 S. Jose, A. S. Aprem, B. Francis, M. C. Chandy, P. Werner, V. Alstaedt and S. Thomas, Phase morphology, crystallisation behaviour and mechanical properties of isotactic polypropylene/high density polyethylene blends, *Eur. Polym. J.*, 2004, **40**, 2105–2115.
29 P. K. S. Mural, G. Madras and S. Bose, Positive temperature coefficient and structural relaxations in selectively localized MWNTs in PE/PEO blends, *RSC Adv.*, 2014, **4**, 4943–4954.
30 P. K. S. Mural, M. S. Rana, G. Madras and S. Bose, PE/PEO blends compatibilized by PE brush immobilized on MWNTs: improved interfacial and structural properties, *RSC Adv.*, 2014, **4**, 16250–16259.
31 S. Bose, C. Özdilek, J. Leys, J. W. Seo, M. Wübbenhorst, J. Vermant and P. Moldenaers, Phase Separation as a Tool to Control Dispersion of Multiwall Carbon Nanotubes in Polymeric Blends, *ACS Appl. Mater. Interfaces*, 2010, **2**, 800–807.
32 G. Vleminckx, S. Bose, J. Leys, J. Vermant, M. Wübbenhorst, A. A. Abdala, C. Macosko and P. Moldenaers, Effect of Thermally Reduced Graphene Sheets on the Phase Behavior, Morphology, and Electrical Conductivity in Poly [(α-Methyl Styrene)-*co*-(Acrylonitrile)/Poly(Methyl-Methacrylate) Blends, *ACS Appl. Mater. Interfaces*, 2011, **3**, 3172–3180.
33 C. Marambio-Jones and E. M. Hoek, A review of the antibacterial effects of silver nanomaterials and potential implications for human health and the environment, *J. Nanopart. Res.*, 2010, **12**, 1531–1551.
34 A. Muñoz-Bonilla and M. Fernández-García, Polymeric materials with antimicrobial activity, *Prog. Polym. Sci.*, 2012, **37**, 281–339.

35 M. Sharma, G. Madras and S. Bose, Unique nanoporous antibacterial membranes derived through crystallization induced phase separation in PVDF/PMMA blends, *J. Mater. Chem. A*, 2015, **3**, 5991–6003.

36 Y. Zhu, M. D. Stoller, W. Cai, A. Velamakanni, R. D. Piner, D. Chen and R. S. Ruoff, Exfoliation of Graphite Oxide in Propylene Carbonate and Thermal Reduction of the Resulting Graphene Oxide Platelets, *ACS Nano*, 2010, **4**, 1227–1233.

37 C. Baker, A. Pradhan, L. Pakstis, D. J. Pochan and S. I. Shah, Synthesis and antibacterial properties of silver nanoparticles, *J. Nanosci. Nanotechnol.*, 2005, **5**, 244–249.

38 J. S. Taurozzi, H. Arul, V. Z. Bosak, A. F. Burban, T. C. Voice, M. L. Bruening and V. V. Tarabara, Effect of filler incorporation route on the properties of polysulfone–silver nanocomposite membranes of different porosities, *J. Membr. Sci.*, 2008, **325**, 58–68.

39 M. J. Hajipour, K. M. Fromm, A. Akbar Ashkarran, D. Jimenez de Aberasturi, I. R. d. Larramendi, T. Rojo, V. Serpooshan, W. J. Parak and M. Mahmoudi, Antibacterial properties of nanoparticles, *Trends Biotechnol.*, 2012, **30**, 499–511.

40 C. D. Vecitis, K. R. Zodrow, S. Kang and M. Elimelech, Electronic-Structure-Dependent Bacterial Cytotoxicity of Single-Walled Carbon Nanotubes, *ACS Nano*, 2010, **4**, 5471–5479.

41 J. R. Morones, J. L. Elechiguerra, A. Camacho, K. Holt, J. B. Kouri, J. T. Ramírez and M. J. Yacaman, The bactericidal effect of silver nanoparticles, *Nanotechnology*, 2005, **16**, 2346.